Rare Metal Materials and Engineering
Volume
Available online at **www.rmme.ac.cn**

Science Press

Cite this article as: Rare Metal Materials and Engineering,

ARTICLE

https://doi.org/10.12442/j.issn.1002-185X.20250607

The Corrosion Behavior of Pre-oxidized 56Cu-22Ni-12Fe-8Al-2La Anode Alloy in Low Temperature Molten Electrolyte for Aluminum Electrolysis

Juan Du[1,2], Shengzhong Bao[3], Shaodan Yang[1,2], Yanjun Zhou[2,4], Yuwei Zhuang[5], Shuguang Cao[1]

[1]Institute of Materials, Henan Academy of Sciences, Zhengzhou, 450046, China; [2] Henan Key Laboratory of Advanced Conductor Materials, Zhengzhou, 450002, China; [3] Zhengzhou Non-ferrous Metals Research Institute Co. Ltd of CHINALCO, Zhengzhou, 450041, China; [4] School of Material Science and Engineering, Henan University of Science and Technology, Luoyang, 471023, China; [5] High&New Technology Research Center of Henan Academy of Sciences, Zhengzhou, 450046, China

Abstract: The corrosive behaviors of unoxidized and pre-oxidized 56Cu-22Ni-12Fe-8Al-2La anode alloys are investigated in Na_3AlF_6-K_3AlF_6-AlF_3-Al_2O_3 electrolytes for aluminum electrolysis at 800℃. Results show that the oxide layer formed on the pre-oxidized alloy at 800 ℃ under O_2 atmosphere is mainly oxides of aluminum, nickel, iron, copper, and lanthanum. After 3h aluminum electrolysis, the corrosion products formed on unoxidized anode alloy is a tri-layered structure and the discontinuous and porous oxide layer provides a connected channels during electrolysis, allowing direct electrolyte penetrate into the metal matrix for about 320 μm thickness. The corrosion oxide layer formed on pre-oxidized anode alloy is about 190 μm thickness. The out and inner oxide layer includes a continuous Ni/Fe/Al/Cu-rich (mainly $NiFe_2O_4$, $CuAlO_2$) oxides. The middle layer containing of a dense and continuous $NiFe_2O_4$ with a thickness about 15 μm. A small amount of electrolyte appears in the oxide layer and penetrate into the metal matrix. The pre-oxidized alloy exhibited a better corrosion resistance and stability in comparison with that unoxidized alloy during aluminum electrolysis. The electrochemical performances testing of the metal anodes in molten salt for aluminum electrolysis are carried out and the corrosion mechanism of the alloys are also investigated.

Key words: Cu–Ni–Fe-Al-La alloy, Metal anodes, High temperature corrosion, molten electrolyte

The aluminium production is usually carried out by the conventional Hall-Héroult process[1,2]. However, the high energy consumption and emission of greenhouse gases of Hall-Héroult process produces a large adverse impact on the environment [3,4]. Developing non-carbon inert anodes for aluminum electrolysis offers an effective approach to addressing this issue. I. Gallino[5], Wenjie Yang[6] and Zhaowen Wang[7] have employed Cu-Fe-Ni and Fe-Ni alloy as inert anode material for aluminum electrolysis, respectively. $NiFe_2O_4$-based cermet[8-10] and (Cu, Ni)/(10NiO-$NiFe_2O_4$) conducting ceramic[11-13] have also been investigated as anode materials in aluminum electrolysis. As an alternative material to carbon anodes in the modern electrolytic aluminium industry, metallic-based inert anodes exhibit several advantages, such as high strength, excellent electrical conductivity, strong resistance to thermal shock, ease of processing and shaping, and the ability to achieve connections with metal conductor rods [14,15]. Copper or nickel-based alloys such as Cu-Ni-Fe [16,17], Cu-Al [18,19] and Ni-Fe [20,21] are mainly metallic anode materials because of the capability of forming corrosion resistant oxide layers during the molten salt electrolysis process. The formation of a dynamic balance resistant oxide layer on

Received date:
Foundation item: The Scientific Research Start-up Fund of Henan Academy of Sciences (231817003); Natural Science Foundation of Henan Province (242300420030); High-level Achievement Award and Cultivation Project of Henan Academy of Sciences (20252317003); Key R&D and Promotion Special Project (Science and Technology Research) of Henan Province (242102230031); Innovation Team Project of Henan Academy of Sciences (20250104); The Fundamental Research Fund of Henan Academy of Sciences (240617039).
Corresponding author: Juan Du, Ph. D., Professor-level Senior Engineer, Institute of Materials, Henan Academy of Sciences, Zhengzhou 450046, P. R. China, Tel: 15937116263, E-mail: juan_du@hnas.ac.cn

anodic surface is the key point of preparing a qualified metal anode.

T.R. Beck et al.[15] and Dao Cao et al.[24] demonstrated that the formation of an adherent and electronically conductive $NiFe_2O_4$ layer in the passive film after electrolytic oxygen evolution significantly enhanced the corrosion resistance of Cu-Ni-Fe alloys and Ni-Fe anodes in molten fluoride salts. S. Helle et al.[25] have studied the corrosion behavior Cu-Al-Ni-Fe alloy in a 700°C KF-AlF_3 melt. The results showed that a $CuAl_2O_4$ protective layer formed on the substrate surface effectively prevented the penetration of the electrolyte and the spalling of oxides. Zhongliang Tian[13] and Wenjie Yang et al.[26] have proved that the a continuous and dense $FeAl_2O_4$, $NiAl_2O_4$, $CuAl_2O_4$ or $NiFe_2O_4$ film derived from the metal phase in the cermet would provide excellent protection to the internal structure of the anode during the electrolysis process. However, the $NiFe_2O_4$ and metal aluminates protective scales are usually fragile and exist poor adhesion with the alloy substrates. These characteristics would lead to the failure of anode during the aluminum electrolysis process rapidly. Therefore, improving the adhesion between the protective layer and the alloy substrate is essential to obtain a stable and corrosion resistant metal anodes during the electrolysis in molten salts.

Besides, some researchers have stated that pre-oxidizing the metal alloys also can improve the corrosion resistance. Wei wei et al.[27] studied that after the oxidation at 960℃ in air of Ni-Fe-15Cr alloy, a tri-layer oxide structure with an outer layer of (Ni, Fe)$_3O_4$ spinel, a middle layer of (Ni, Fe, Cr)$_3O_4$ spinel and an oxidation resistant inner layer of Cr_2O_3 were formed on the alloy surface. Simultaneously, the tri-layer oxide scale exhibited good electrical property and corrosion resistance in aluminum electrolysis process. Reza Tamasgavabari et al.[28] examined the corrosion behavior of a Ni-6Al-10Cu-11Fe-15Cr nickel-based alloy as an inert anode material in a cryolite melt. The study found that the addition of Al and Cr to the alloy composition played an important role in delaying the corrosion of the metal alloys by the molten salt electrolyte, due to the formation of Al_2O_3 and Cr_2O_3 after pre-oxidation. Kamaljeet Sing et al.[29] have studied Cu-Ni-Fe alloys as anodes in a low-temperature laboratory aluminum electrolysis cell. It is found that the pre-formed oxide layer remains compact post-electrolysis through oxidation treatment on the alloy. However, it remains a great challenge for metal alloys surviving in the high-temperature (960℃) corrosion condition of NaF-AlF_3 cryolite molten salt for a long time.

Based on those requirements above on metallic anode alloys, developing an improving adhesion and corrosion resistant oxide layer on anode surface is desirable for aluminum electrolysis. According to our previous study, the addition of La could peg in the grain boundary and improve the oxidation resistance and adhesion of the oxide film.[30] The pre-oxidation may promote the homogenization of the alloys' microstructure and the formation of oxide layer.[20] Therefore, in this article, both aluminum (Al) and lanthanum (La) elements are added into the copper-nickel-iron (Cu-Ni-Fe) alloy, following a pre-oxidation pretreatment. In particular, a low-temperature KF-NaF-AlF_3-based electrolyte with high alumina solubility is employed here to offer a better service condition for the metal anodes. Until now, there is limited research on the electrochemical corrosive behavior of pre-oxidized and the multi elements-regulated Cu-Ni-Fe alloy during aluminum electrolysis. Especially, the evolution of the pre-oxidized film and the corrosion mechanism of the Cu-Ni-Fe-Al-La alloy have not been revealed yet in the low-temperature KF-NaF-AlF_3 based electrolyte.

In this paper, a pre-oxidized Cu-Ni-Fe-Al-La alloy as the anode material is prepared for aluminum electrolysis. The electrochemical performances of the pre-oxidized Cu-Ni-Fe-Al-La alloy are investigated under the galvanostatic electrolysis in Na_3AlF_6-K_3AlF_6-AlF_3-Al_2O_3 electrolyte at 800 °C. For comparation, the corrosion behaviors of the Cu-Ni-Fe-Al-La with and without pre-oxidized are evaluated and discussed.

1 Experiment

1.1 Sample preparation

The 56Cu-22Ni-12Fe-8Al-2La alloys were fabricated from high purity (>99.9%) of copper, nickel, iron and copper-lanthanum master alloy by high frequency induction melting under argon atmosphere. During the melting and casting process, electromagnetic stirring is used to get a good ingot with high quality. The test samples were cutted into cylindrical bars with a diameter of 8.5 mm and 7 mm at length from the ingot by electrodischarge machine. Prior to pre-oxidation, the samples were abraded with SiC-paper upto 2000 grit. After washed in water and ultrasonically degreased in ethanol. Finally, the dried samples were preoxidized at 800°C under an O_2 atmosphere for 100 hours.

1.2 Galvanostatic Electrolysis and Electrochemical Test

For comparation, the pre-oxidized and unoxidized samples were chosen to take aluminum electrolysis tests in a three-electrode cell at 800°C for 3h. The anode current density of 0.5 Acm^{-2} were performed in a mixing cryolite with NaF (20 wt.%), KF (20.27 wt.%), AlF_3 (51.74% wt.%), and Al_2O_3 (8 wt.%). A laboratory electrolytic cell was set up within a vertical furnace, as shown in Fig.1. A high purity graphite crucible used as the cathode was in a corundum crucible sealed with a stainless steel lid. The stainless steel sealing lid has gas inlet and outlet holes to allow inert gas flow. The bottom of a cylindrical anode sample (the test area d=7.5mm, h=7mm) was threaded into a boron nitride disc, and the top of the anode sample was connected to the power supply with a corundum as a protected sleeve. High purity aluminum in a corundum crucible with a 1.5mm diameter hole on the bottom was

employed as the reference electrode. A tungsten wire was served as the current collector for the reference electrode.

The anode and reference electrodes on the boron nitride disc were suspended above the electrolyte at the beginning of heating. The temperature of the electrolysis cell was raised to 250°C holding for 2 hours, followed by further heating to 800°C at a rate of 5°C min^{-1}, holding for 0.5 hours. After the electrolyte was fully melted, the anode was put down and immersed 2 cm below the electrolyte surface. Open-circuit potential (OCP) was measured for 1 hour by an electrochemical workstation (IM6, Zahner). Then, the galvanostatic electrolysis was carried out at the current density of 0.5 A cm^{-2} for 3 hours. During electrolysis, electrochemical impedance spectroscopy (EIS) measurements were conducted hourly with a perturbation amplitude of 10 mA and the frequency range was from 5 kHz to 0.1 Hz. Upon completion of electrolysis, the anode material was raised above the molten salt electrolyte. After cooling to room temperature under an inert gas atmosphere, the sample was retrieved for microstructural analysis. The linear sweep voltammetry curves are also measured after EIS measurement on parallel samples following same procdures descripted as above. The scan range is from the open circuit potential to 2.8 V vs. Al/Al^{3+} with a scan rate of 0.001Vs^{-1}.

1.3 Microstructure characterization

After electrolysis, the samples were encapsulated in epoxy resin to secure the corrosion product layer against detachment. The cross-section was ground with 600#, 800#, and 1200# abrasive papers. After grinding, the samples were rinsed with deionized water and ethanol to remove residual abrasives, subsequently dried. The phase structure of the oxide scale was identified by X-ray diffraction (XRD, PANalytical X'pert Pro) with Cu-Kα radiation scanned in the 2θ range of 10-90° under conditions of 40 kV and 40 mA. The surface morphologies and cross-sections of the samples after electrolysis were characterized by scanning electron microscopy (SEM, JEOL JSM-6360LV) with an energy dispersive X-ray spectroscopy (EDS, Oxford-INCA).

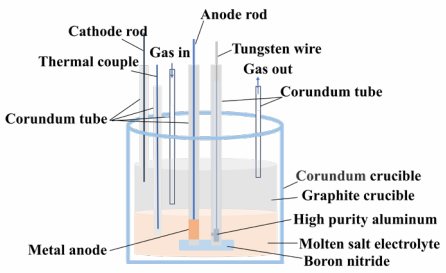

Fig.1 Schematic diagram of electrolysis cell

2 Results and Discussion

2.1 Microscopic Morphology and Element Analysis of the Anode Alloy After Pre-Oxidation

Fig.2 presents a scanning electron microscopy (SEM) image and elemental analysis (EDS) of the cross-section of the 56Cu-22Ni-12Fe-8Al-2La alloy after pre-oxidized at 800°C for 100 hours under an O_2 atmosphere. The results demonstrate that the formation of an oxide layer extending approximately 30 μm beneath the material surface. This oxide layer is mainly composed of oxides of aluminum, nickel, iron, copper, and lanthanum. Especially, the oxide of aluminum is the predominate product. To some extent, the formation of this oxide layer can prevent the rapid erosion of the metal anode by the electrolyte at the initial immersion period [28, 31, 32].

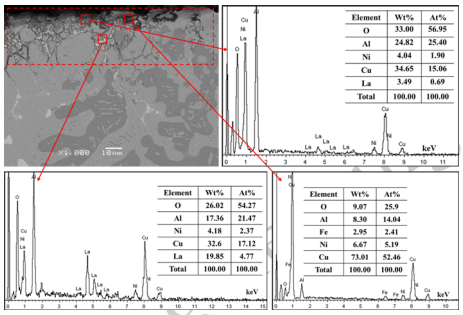

Fig.2 The cross section of the pre-oxidized 56Cu-22Ni-12Fe-8Al-2La alloy (SEM and EDS)

2.2 Corrosion Behavior of Anode Alloy in Aluminum Electrolysis Process

2.2.1 The Open Circuit Potential (OCP) and Electrolytic Voltage Testing

For comparation, both pre-oxidized and unoxidized alloys are used as anode materials in the electrolysis experiments for electrochemical performances testing. Figures 3a is the open-circuit potential variation for the pre-oxidized and unoxidized metal anode materials after immersion in the electrolyte for 1h. It demonstrates that the OCP of the pre-oxidized anode alloy is significantly higher than that of the unoxidized anode material during the initial immersion in the electrolyte. This is mainly attribute to the formation of a pre-oxidized layer on the surface of the anode alloy. At the initial stage of immersion in the electrolyte, this pre-oxidized layer serves as a protective barrier that effectively slow down the erosion of the high-temperature electrolyte on the metal substrate.

Fig.3b shows the electrolysis voltage as function of electrolysis time for both anode alloys. It is clear that the electrolysis voltages of both anode alloys rise sharply from a starting value of 0.4 to 2.5 V in the first 6 min of electrolysis. This period is assumed to the electrochemical oxidation of the anodes dominantly [33]. Subsequently, the electrolysis voltage increases slowly to reach around 2.7 V at the end of electrolysis. This may be due to the fact that the anode alloys have nearly reached the steady electrolysis state, such as a balance between the respective rates of oxide formation and dissolution have established [34,35]. It is note that the electrolysis voltage

for pre-oxidized anode alloy is a slightly higher about (0.03V) than the unoxidized anode alloy after 100 min electrolysis. The oxidized layer thermally developed on 56Cu-22Ni-12Fe-8Al-2La has an acceptable anode resistance for Hall-Héroult aluminum electrolysis process.

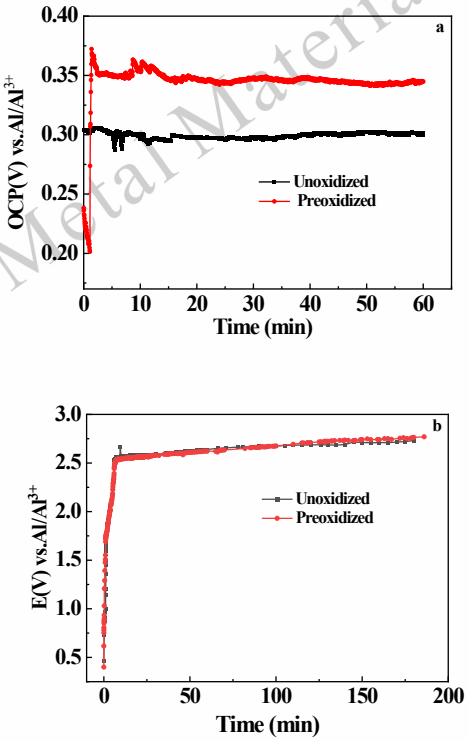

Fig.3 a-The variation of OCP for pre-oxidized and unoxidized anode alloys within the first hour of immersion in the electrolyte
b-The electrolytic voltage as function of time for pre-oxidized and unoxidized anode alloys

2.2.2 The Analysis for the Corrosion Products

The cross-section of the unoxidized and pre-oxidized anode metals are analyzed by SEM and EDS, as show in Fig.4. Clearly, both the surface of unoxidized and pre-oxidized anode metals are covered by a layer of solidified electrolyte. For unoxidized anode (Fig.4a), the thickness of surface oxide is approximately 160 μm. Besides, between the metal substrate and the oxide layer, there is an electrolyte penetration area with a thickness of approximately 320 μm, the total thickness of the corrosion zone is about 480 μm. In comparison, the original aluminum oxide predominated layer formed on the pre-oxidized anode metal have converted into a dense mixed oxide layer. The mixed oxide layer thickness is approximately 190 μm, and the thickness of electrolyte penetration area is about 130 μm, the total thickness of the corrosion zone is about 320 μm (Fig.4b).

To further investigate the detailed composition of the oxide layer, the EDS elements point and line scans are carried out on the cross section of the anode metals. The X-Ray diffraction analysis results are also presented in Fig.5. It is demonstrated that the surface of unoxidized and peroxidized alloy anodes after 3h electrolytic corrosion mainly contains oxide (Cu_2O, NiO), spinel ($NiFe_2O_4$, $CuAlO_2$) and potassium/sodium/aluminum fluoride (KF_3, NaF_3, AlF_3) phases. In order to provide a clearer representation of the results, an attempt is made to simplify the depiction of various phase of the oxide layers, as shown in Fig.6. For unoxidized 56Cu-22Ni-12Fe-8Al-2La anode, as shown in Fig.6a, the surface oxide is composed of a tri-layered oxide structure with an outer layer of Cu oxide (mainly Cu_2O), a middle layer is a discontinuous $NiFe_2O_4$, Al_2O_3 and an inner layer of a porous Ni/Fe/Al -rich hybrid oxides. Obviously, the discontinuous and porous oxide layer provides a connected channels during electrolysis, allowing direct electrolyte contact with the anode metal matrix, ultimately expanding into about 320 μm thickness electrolyte penetration zones. Obviously, the electrolyte preferentially penetrates along La-enriched regions toward the metal substrate. It is attributed to the La may reduce the grain boundary energy at segregation sites and react with electrolyte ($La + AlF_3 \rightarrow LaF_3 + Al$) during aluminum electrolysis.[36] The penetrated electrolyte may give rise to the microlocal corrosion of the metal anode, resulting in the degradation of the mechanical properties of the oxide layer and even making the oxide layer easily exfoliated.

In contrast, for the pre-oxidized metal anode, the oxide layer is about 190 μm thick and also consisted of three-layer structure (Fig.6b). Both the out and inner oxide layer includes a dense and continuous Ni/Fe/Al/Cu-rich (mainly $NiFe_2O_4$, $CuAlO_2$) oxides with a small amount of electrolyte. The middle layer containing of a dense and continuous Ni/Fe-rich ($NiFe_2O_4$) with a thickness about 15 μm. Apparently, the no damaged $NiFe_2O_4$ layer together with the dense Ni/Fe/Al/Cu-rich (mainly $NiFe_2O_4$, $CuAlO_2$) oxides can offer superior corrosion resistance in cryolite-alumina molten electrolyte. The formation of dense and continuous $NiFe_2O_4$ layer and Ni/Fe/Al/Cu-rich oxides layer may attribute to the homogeneous microstructure be obtained by the high temperature pre-oxidized. Moreover, the outward diffusion of Cu is restrained due to the homogeneous structure and the formation of $NiFe_2O_4$ is promoted by the homogenization treatment [20]. It is worth noting that a small amounts of F, Al and K appears in the oxide layer and penetrate into the metal matrix. It is evident that the oxide layer formed on the pre-oxidized anode exhibited a better corrosion resistance and stability in comparison with that on unoxidized anode after aluminum electrolysis of 3h. It is note that the delamination of oxide layer occurred for pre-oxidized alloy anode after 3h electrolysis. However, the whole oxide layer is not damaged at all. Since only a little electrolyte is present in the Ni/Fe/Al/Cu-rich oxides rather than fully filling between metal matrix and oxide layer, it is not possible for the oxide layer to delamination during electrolysis. The oxide layer delamination is probably due to the thermal “shock” when the metal anode was raised

above the molten electrolyte after electrolysis. Besides, the difference in the coefficients of thermal expansion between the alloy substrate and the oxide layer may also generate the delamination [31,37].

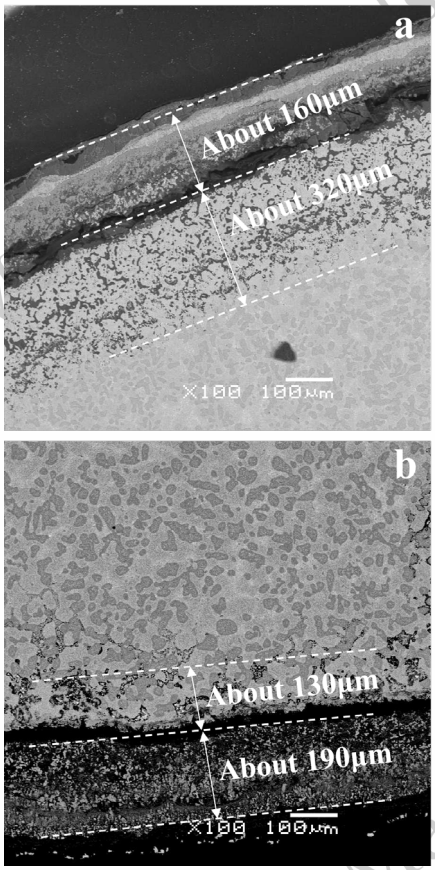

Fig.4 Cross-sectional SEM/BSE images of scales on unoxidized (a) and pre-oxidized (b) 56Cu-22Ni-12Fe-8Al-2La alloys after 3h of electrolysis at 800 °C

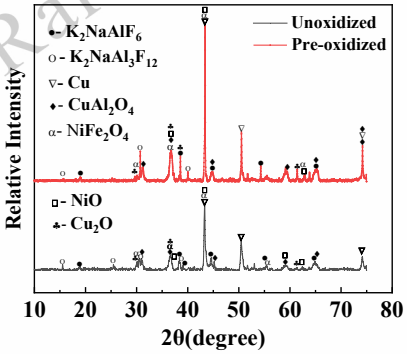

Fig.5 X-Ray diffraction patterns for the oxide layers with respect to unoxidized and pre-oxidized alloy after 3h electrolysis

2.3 Corrosion Mechanism of the Unoxidized and Pre-oxidized Anode alloys

Fig.7 shows the linear sweep voltammetry curves of the unoxidized and pre-oxidized in the molten salt at 800℃. The scan range is from the open circuit potential to 2.8 V vs. Al/Al^{3+} with a scan rate of $0.001Vs^{-1}$. Fig.7 shows the linear sweep voltammetry curves of the unoxidized and pre-oxidized in the molten salt at 800℃. The scan range is from the open circuit potential to 2.8 V vs. Al/Al^{3+} with a scan rate of $0.001Vs^{-1}$. Obviously, the polarization current density of pre-oxidized anode is observed to be slightly lower than that of unoxidized anode proving a little better corrosion resistance of the pre-oxidized anode alloy. The linear sweep voltammetry curves of the both alloys are divided into four stages. In order to interpretate the reaction occurring on the alloys surface at different potential range, the electromotive series for aluminum electrolysis at 1100 K are also calculated based on free energies of formation of compounds in JANAF thermochemical tables.[15, 38, 39] In AB stage, the current density increases with a positive shift of the potential indicating the alloy is dissolved and reacts with the molten salts corresponds to the active dissolution of the alloy, especially La element.

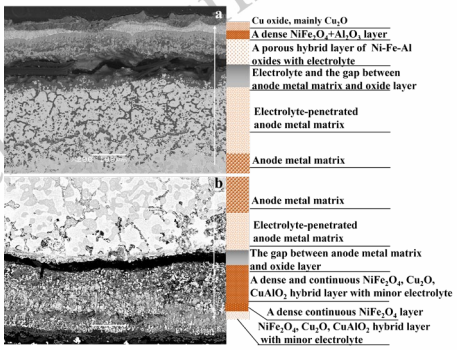

Fig.6 SEM image of the cross-section of unoxidized (A) and pre-oxidized (B) samples after 3h of electrolysis at 800 °C.

$$La + F^- \rightarrow LaF_3 \qquad E = 0.71\ V\ vs.\ Al/Al^{3+} \qquad (1)$$

The BC and DE stages represent the passivation transition zone. The decrease of current densities in passivation transition zone is attributed to the metal elements start to convert from the activated state to passivated state leading to the oxide protective layers gradually formed on the anode surfaces. In CD stage, the current densities of unoxidized and pre-oxidized alloys both increase gradually indicating the dissolution of the metallic elements at the specific potential [25]. The predominant reactions occurring at CD may involve the following reactions[43]:

$$Fe + Al_2O_3 \rightarrow Fe_2O_3 + Al \quad E^0 = 1.37\ V\ vs.\ Al/Al^{3+} \qquad (2)$$

$$Ni + Fe + Al_2O_3 \rightarrow NiFe_2O_4 + Al \quad E^0 = 1.396\ vs.\ Al/Al^{3+} \qquad (3)$$

$$Ni + AlF_3 \rightarrow NiF_2 + Al \quad E^0 = 1.71 vs.\ Al/Al^{3+} \qquad (4)$$

$$Cu + Al_2O_3 \rightarrow Cu_2O + Al \quad E^0 = 1.84\ vs.\ Al/Al^{3+} \qquad (5)$$

$$Cu + Al_2O_3 \rightarrow CuO + Al \quad E^0 = 1.99\ vs.\ Al/Al^{3+} \qquad (6)$$

$$Cu + AlF_3 \rightarrow CuF_2 + Al \quad E^0 = 2.06\ vs.\ Al/Al^{3+} \qquad (7)$$

$$Al_2O_3 + AlF_3 \rightarrow Al_xO_yF_z + Al \quad E^0 = 2.07V\ vs.\ Al/Al^{3+} \qquad (8)$$

$$Cu_2O + Al_2O_3 \rightarrow CuO + O_2 + Al \quad E^0 = 2.25V\ vs.\ Al/Al^{3+} \qquad (9)$$

$Cu + AlF_3 \rightarrow CuF_2 + Al$ E^0=2.3 vs. Al/Al^{3+} (10)

$Al_2O_3 \rightarrow Al + O_2$ E^0=2.351 V vs. Al/Al^{3+} (11)

However, it is noted that pre-oxidized alloy exhibits three dis tinct current plateaus in the CD stage. This phenomenon is may due to the homogenized microstructure induced by pre-oxidation, facilitating the development of dense, continuous and stable passivated oxide layers at the potential between 0.73 to 2.09 V vs Al/Al^{3+}. Comparatively, the current density for unoxidized anode alloy in the CD stage continuously increases to about 1.7 V vs Al/Al^{3+} to appear a small current plateaus. Besides, the current peak observed at 2.3 V vs Al/Al^{3+} of unoxidized alloy may be attributed to the formation of CuO and CuF_2 (Reaction 9 and 10), indicating that the electrochemical polarization formed oxide layer is not effectively to block fluoride ion penetrate to the metal matrix. Whereas, for pre-oxidized anode alloy, a better passivated oxidized layer formed during the electrochemical polarization process suppresses further penetration of fluoride ion and avoid the reaction of fluoride ion and metal substrate at 2.3V vs Al/Al^{3+}. Finally, at the EF segment, the alumina begins to decompose with the oxygen evolution from the breakdown potential (E_b, E'_b), and the current density increases with increasing potential.

Additionally, the linear sweep voltammetry curves give several characteristic potentials and currents important for evaluating the passivation behavior of alloys in molten salt. A more negative passivation potential (E_p, E'_p) indicates a greater tendency for the metal enters the passivation state. Obviously, the E'p1, E'p2 values of the pre-oxidized alloy is more negative than unoxidized alloys (E_{p1}, E_{p2}), indicating that it becomes easier to enter the passivation state.

In order to further investigate the corrosion resistance of unoxidized and pre-oxidized anode alloys in the molten electrolyte, electrochemical impedance spectra (EIS) tests have been performed after the OCP of anode alloys are stable in the molten electrolyte for about 1h. The results are displayed in forms of both Nyquist and Bode plots in Figure 8(a) and Figure(b, c). As is known, for the metal corrosion, the Nyquist plot usually consists of three regions that are dependent on the frequency range. At a high frequency, the nonzero intercept of the real axis indicates the equivalent series resistance (R_s) of a system, and R_s is mainly the combination of the bulk resistance of an electrolyte solution. In a medium-frequency region, electrochemical behavior related to the interfacial charge transfer resistance of an electrode/electrolyte system is attributed to the capacitive behavior of electrodes. The low-frequency domain represents diffusion properties due to electrode porosities and surface states. After 1h of immersion, the Nyquist plots for both anode alloys feature a high-frequency R_s, a medium-frequency capacitive arc and a low-frequency impedance arc with Warburg characteristics. To elucidate the corrosion process from the EIS, the impedance spectra are fitted using the equivalent circuit in Figure 8(b). Where L represents the inductance, R_s is the solution resistance, considering that the corrosion interface of metal anodes may exhibit defects rather than an ideal smooth surface, there have an electrochemical effect in metal/solution interface. A constant phase element (CPE) is commonly used to replace an ideal capacitance element (C), R_{ct} is the charge transfer resistance, and W_s is Warburg diffusion[40-42]. Table 1 summarizes the fitted equivalent circuit parameters results.

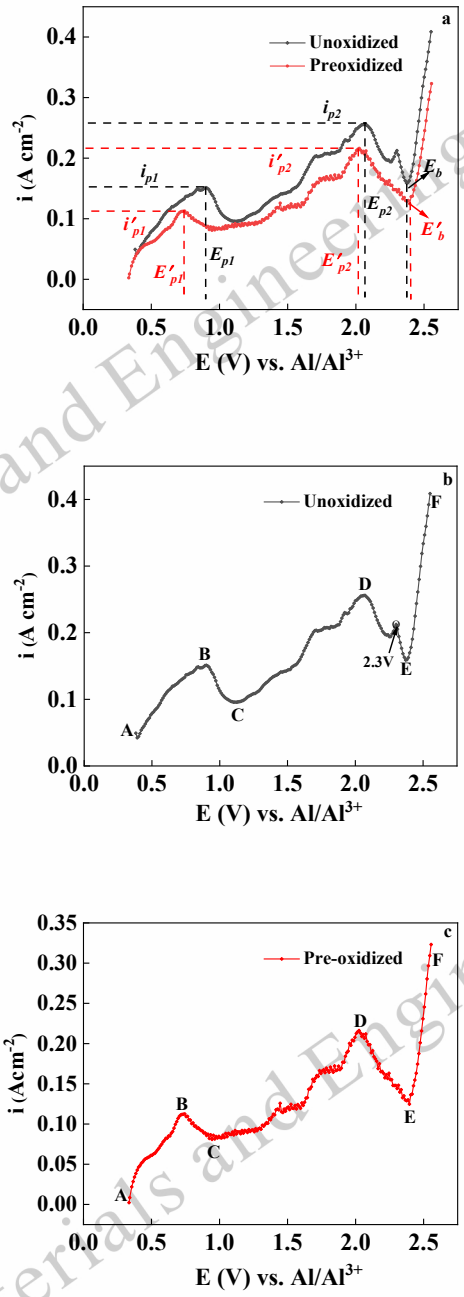

Fig. 7 Anodic polarization curves (a) of unoxidized (b) and pre-oxidized (c)anode alloys in aluminum electrolysis molten at 800℃

Table 1 Impedance parameters of unoxidized and pre-oxidized anode alloys after immersing in aluminum electrolysis molten electrolyte for 1 h

Anode alloy	L_A(H)	R_s (Ω/ cm^2)	R_t (Ω/ cm^2)	C_{dl} (F/cm^2)	β	W (Ω/cm^{2}S$^{0.5}$)
Unoxidized	762.7n	157.8m	50.4m	201.3m	0.5599	130.6m
Pre-oxidized	2.052μ	128.2m	68.2m	230.9m	0.6036	177.3m

A higher R_{ct} for pre-oxidized than unoxidized anode alloy indicates that the oxide products formed by pre-oxidization on 56Cu-22Ni-12Fe-8Al-2La alloy may impede ion-substrate interactions at the initial immersion stage in molten electrolyte. Besides, a higher Warburg impedance of pre-oxidized alloy than unoxidized alloy represent a lower diffusion of the electrolyte to the pre-oxidized alloy surface. It is further confirmed that the pre-formed oxide film can provide partial barrier protection against electrolyte diffusion and corrosion attack on the metal substrate for pre-oxidized anode alloy. The EIS measurements of unoxidized and pre-oxidized anode alloys at various galvanostatic electrolysis durations are also carried out (Supporting information Figure S5). It is observed that the R_s gradually increases with extending the galvanostatic electrolysis duration. However, the data at low-frequency exhibit irregularities due to the evolution of oxygen bubble during electrolysis. Accordingly, these EIS results are not presented and discussed here.

Finally, it should be noted that long-term electrolysis or large current density may probably alter the 56Cu-22Ni-12Fe-8Al-2La anode alloy performances significantly. The purpose of this study is not to identify this anode alloy with suitable long-term stability, but rather to reveal the effect of pre-oxidation on the corrosion behavior of the 56Cu-22Ni-12Fe-8Al-2La during the initial electrolysis process.

Therefore, in the future, a long-term electrolysis should be carried out in a 20A, 200A laboratory cell for 24h to 72h electrolysis. Subsequently, if this metallic anode exhibits a good performance, a 20kA electrolysis experiment may be further conducted to evaluate the performance of the metallic anode and the comprehensive performance of the total electrolysis cell, thereby providing reliable data supporting for the industrial application of the metallic anodes.

3 Conclusions

1) The oxide layer formed on 56Cu-22Ni-12Fe-8Al-2 La alloy at 800 °C under an O_2 atmosphere is mainly composed of oxides of aluminum, nickel, iron, copper, and lanthanum. Especially, the oxide of aluminum is the predominate product. To some extent the formation of this oxide layer can prevent the rapid erosion of the metal anode by the electrolyte at the initial immersion period.

2) After 3h aluminum electrolysis, the oxide formed on surface of unoxidized 56Cu-22Ni-12Fe-8Al-2La anode is composed of a tri-layered oxide structure with an outer layer of Cu oxide (mainly Cu_2O), a middle layer is a discontinuous

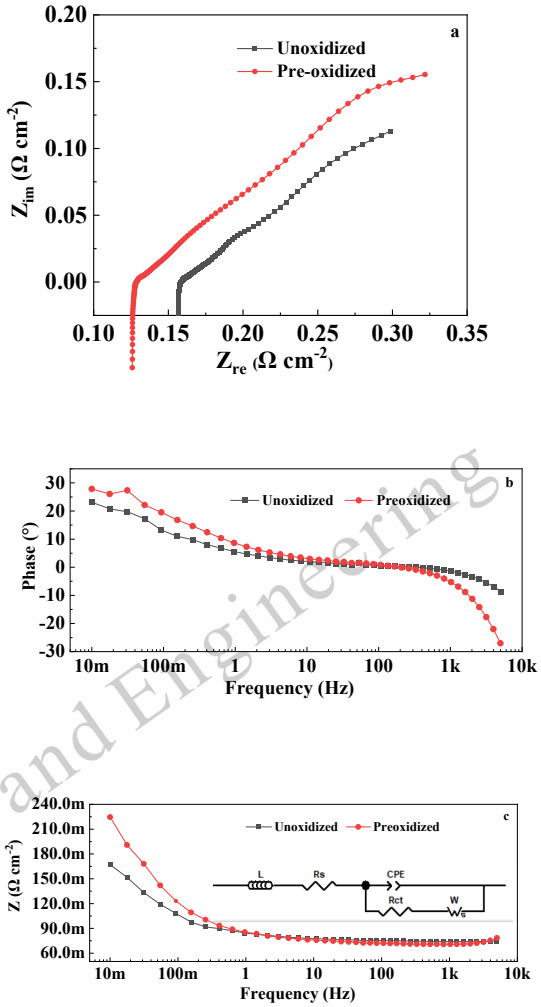

Figure 8 Nyquist plots (a), and Bode plots (b, c) The illustration here represents an equivalent circuit) of the three alloys after immersion in aluminum electrolysis molten for 1h at 800℃

$NiFe_2O_4$, Al_2O_3 and an inner layer of a porous Ni/Fe/Al -rich hybrid oxides. The discontinuous and porous oxide layer provides a connected channels during electrolysis, allowing direct electrolyte contact with the anode metal matrix, ultimately expanding into about 320 μm thickness electrolyte penetration zones. The electrolyte preferentially penetrates along La-enriched regions toward the metal substrate. The penetrated electrolyte may give rise to the microlocal corrosion of the metal anode, resulting in the degradation of the mechanical properties of the oxide layer and even making the oxide layer easily exfoliated.

3) For the pre-oxidized metal anode, the oxide layer is about 190 μm thickness and also consisted of three-layer structure. Both the out and inner oxide layer includes a dense and continuous Ni/Fe/Al/Cu-rich (mainly $NiFe_2O_4$, $CuAlO_2$) oxides with a small amount of electrolyte. The middle layer containing of a dense and continuous Ni/Fe-rich (NiFe2O4)

with a thickness about 15 μm. A small amount of F, Al and K appears in the oxide layer and penetrate into the metal matrix. It is evident that the oxide layer formed on the pre-oxidized anode exhibited a better corrosion resistance and stability in comparison with that on unoxidized anode after aluminum electrolysis of 3h.

In summary, firstly, compared with the nickel-iron series or copper-nickel-iron series metallic anodes, the metallic anode developed in this study, via the co-doping of aluminum and rare earth element as well as high-temperature pre-oxidation treatment, can more prone to form a dense and continuous oxide layer (e.g., nickel ferrite, nickel aluminate) in molten salt electrolytes. These metal oxide layers with self-healing capability exhibit excellent resistance to molten salt corrosion and erosion by molten salt ions. Secondly, cermet anodes are the most widely adopted inert anodes in current pilot-scale aluminum electrolysis experiments. In comparison with cermet anodes, the metallic anode proposed in this study demonstrates more excellent electrical conductivity, thermal shock resistance and workability.

References

1 W. Haupin. History of electrical energy consumption by hall-hiroult cells[M], 1986:106–113.

2 A. P. Ratvik, R. Mollaabbasi, H. Alamdari. ChemTexts[M], 2022, 8:10.

3 P. Desclaux. *Metallurgical and Materials Transactions B*[J], 2001, 32:743.

4 H. Kvande, W. Haupin. *JOM*[J], 2001, 53:29.

5 I. Gallino, M. E. Kassner, R. Busch. *Corrosion Science*[J], 2012, 63:293.

6 W.J. Yang, Y. Wang, H.F. Zhai *et al. Journal of Materials Science*[J], 2020, 55:4065.

7 Z.W. Wang, T. Luo, B.L. Gao, *et al. Rare Metal Materials and Enginerring*[J], 2005, 34:158-161.

8 Z.L. Tian, Y.Q. Lai, Z.Y. Li *et al*. *JOM*[J], 2014, 66:2229.

9 H. Xiao, R. Hovland, S. Rolseth *et al. Metallurgical and Materials Transactions B*[J], 1996, 27:18.

10 H.B. He, Y. Wang, J.J. Long *et al*. *Transactions of Nonferrous Metals Society of China*[J], 2013, 23:381.

11 Z.N. Shi, J.L, B.L. Gao *et al*. *High Temperature Materials and Processes*[J], 2011, 30:247.

12 Y.A. Morozov, V. S. Yalunin. *RUDN Journal of Engineering Research*[J], 2022, 23:15.

13 Z.L. Tian, Y.Q. Lai, S. Yang *et al*. *Metallurgical and Materials Transactions B*[J], 2015, 46:1257.

14 F.L. Sun, X.G. Li, L. Lu et al. *Acta Metallurgica Sinica*[J], 2013, 4:121.

15 T.R. Beck, C. M. Macrae, N. C. Wilson. *Metallurgical and Materials Transactions B*[J], 2011, 42:807.

16 A. S. Yasinskiy, S. K. Padamata, P. V. Polyakov et al. *Transactions of Nonferrous Metals Society of China* [J], 2020, 30:5.

17 P. Sai Krishna, Y. Andrey S, P. Peter V. *Journal of Siberian Federal University. Chemistry*[J], 2018, 11: 18.

18 Y. Liu, D.P Chai, W. Wang *et al*. *Journal of Alloys and Compounds*[J], 2020, 832:154848.

19 S. Helle, B. Brodu, B. Davis *et al*. *Corrosion Science*[J], 2011, 53:3248.

20 P.P. Guan, A.M. Li, Z.N. Shi *et al*. *Metals*[J], 2019, 9: 399.

21 Y.P. Huang, Y.J. Yang, L.M. Zhu *et al*. *International Journal of Electrochemical Science*[J], 2019, 14: 6325.

22 Z.N. Shi, J.L.Xu, Z.X. Qiu *et al*. *JOM*[J], 2003, 55: 63-65.

23 E. N. Zhuravleva, T. N. Drozdova, S. V. Ponomareva *et al. Applied Surface Science*[J], 2013, 265:790.

24 D. Cao, Y.F. Ma, Z.N. Shi *et al. Corrosion Science*[J], 2019, 156:3.

25 S. Helle, B. Davis, D. Guay *et al*. *Journal of the Electrochemical Society*[J], 2010, 15: E173.

26 W.J. Yang, J. Guo, J. Li *et al. Journal of the American Ceramic Society*[J], 2017, 100: 887.

27 W. Wei, S.J. Geng, F.H.Wang. *Journal of Materials Science & Technology*[J], 2022, 107: 216.

28 R. Tamasgavabari, K. Jafarzadeh, M. Madanipoor *et al*. *Anti-Corrosion Methods and Materials* [J], 2015, 62:1.

29 K. Singh, G. Gunnarsson, J.H. Magnusson *et al*. *Journal of The Electrochemical Society*[J], 2023, 170:113507.

30 Y. Liu, Y.A. Zhang, W. Wang *et al. Arabian Journal for Science and Engineering*[J], 2018, 43:6285-6295.

31 W. Wei, S.J. Geng, D.B. Xie *et al. Corrosion Science*[J], 2019, 157: 382.

32 Y. Liu, Z.M. Liang, L.W. *et al*. J*ournal of Hebei University of Science and Technology*[J], 2021, 42: 29.

33 G. Goupil, S. Helle, B. Davis *et al*. *Electrochimica Acta*[J], 2013, *112*: 176.

34 G. Goupil, S. Jucken, D. Poirier *et al*. *Corrosion Science*[J], 2015, *90*: 25.

35 S. Helle, M. Tresse, B. Davis *et al*. *Journal of The Electrochemical Society*[J], 2012, 15: E62.

36 P.Y. Zhang, Z Liu, Z.H. Liu *et al. Special Casting & Nonferrous Alloys*[J], 2024, *44*: 271.

37 B. C. Church, T. H. Sanders, R. F. Speyer *et al. Materials Sci-*

ence and Engineering: A[J], 2007, *452-453*: 334.

38 JANAF Thermochemical Tables, 2nd ed.[M], U.S. National Bureau of Standards, Washington, DC, 1971.

39 S. K. Padamata, A. Yasinskiy, A. Shabanov *et al*. *Transactions of Nonferrous Metals Society of China*[J], 2022, *32*: 354.

40 M. Alzamani, K. Jafarzadeh, A. Fattah-Alhosseini. *Materials and Corrosion*[J], 2019, *70*: 605.

41 C.L. Zeng, W. Wang, W.T. Wu. *Corrosion Science and Protection Technology*[J], 2000, *12*: 249

42 C.S. Ni, L.Y. Lu, C.L. Zeng *et al*. *Corrosion Science*[J], 2011, *53*: 1018.

43 X.K. Qian, C.C. Zhu, X.D. He. *Rare Metal Materials and Enginerring*[J], 2007, 36:1980-1982.

预氧化的 56Cu-22Ni-12Fe-8Al-2La 阳极在铝电解低温熔盐电解质中的腐蚀行为

杜娟[1,2]，包生重[3]，杨少丹[1,2]，周延军[2,4]，庄玉伟[5]，曹书光[1]

(1. 河南省科学院材料研究所，河南 郑州 450046)

(2. 河南省先进导体材料重点实验室，河南 郑州 450002)

（3. 中铝郑州有色金属研究院有限公司，河南 郑州 450041）

（4. 河南科技大学材料与工程学院，河南 郑州 471023）

（5. 河南省科学院高新技术研究中心，河南 郑州 450046）

摘　要：本文研究了未氧化和预氧化的 56Cu-22Ni-12Fe-8Al-2La 金属阳极在 800℃ Na_3AlF_6-K_3AlF_6-AlF_3-Al_2O_3铝电解用熔盐电解质中的腐蚀行为。结果表明，合金在 800℃，O_2气氛下预氧化形成的氧化层主要由铝、镍、铁、铜和镧的氧化物组成。电解 3 小时后，未氧化的金属阳极形成的腐蚀产物呈三层结构，腐蚀产物中分布不连续且多孔的氧化层在电解过程中提供了连通通道，使电解质易直接渗透进入金属基体约 320 μm 深度；预氧化后的金属阳形成的腐蚀产物氧化层厚度约为 190 μm，外层和内层氧化层包含连续的富 Ni/Fe/Al/Cu 氧化物（主要为 $NiFe_2O_4$、$CuAlO_2$），中间层为致密连续的 $NiFe_2O_4$层，厚度约为 15 μm，氧化层中出现少量电解质并渗入金属基体。在铝电解过程中，预氧化后的合金较未氧化的金属阳极合金表现出更优的耐腐蚀性能和稳定性。对金属阳极在铝电解熔盐中的电化学性能进行了测试，并研究了合金的腐蚀机理。

关键词：Cu–Ni–Fe-Al-La 合金, 金属阳极, 高温熔盐腐蚀, 铝电解

作者简介：杜娟，女，1982 年生，博士，正高级工程师，河南省科学院材料研究所，河南 郑州 450046，电话：15937116263，E-mail: juan_du@hnas.ac.cn